Biomedical Optics EXPRESS

Phase-gradient contrast in thick tissue with a scanning microscope

J. Mertz,[1,*] **A. Gasecka,**[2,3] **A. Daradich,**[2,3] **I. Davison,**[4] **and D. Coté**[2,3]

[1]*Boston University, Department of Biomedical Engineering, 44 Cummington St., Boston, MA 02215 USA*
[2]*Centre de Recherche Université Laval Robert-Giffard (CRULRG), Université Laval, Québec, Qc, G1J 2G3, Canada*
[3]*Centre dOptique, Photonique et Laser (COPL), Université Laval, Québec, Qc, G1V 0A6, Canada*
[4]*Boston University, Biology Department, 24 Cummington St., Boston, MA 02215 USA*
[*]*jmertz@bu.edu*

Abstract: It is well known that the principle of reciprocity is valid for light traveling even through scattering or absorptive media. This principle has been used to establish an equivalence between conventional widefield microscopes and scanning microscopes. We make use of this principle to introduce a scanning version of oblique back-illumination microscopy, or sOBM. This technique provides sub-surface phase-gradient and amplitude images from unlabeled tissue, in an epi-detection geometry. That is, it may be applied to arbitrarily thick tissue. sOBM may be implemented as a simple, cost-effective add-on with any scanning microscope, requiring only the availability of an extra input channel in the microscope electronics. We demonstrate here its implementation in combination with two-photon excited fluorescence (TPEF) microscopy and with coherent anti-Stokes Raman scattering (CARS) microscopy, applied to brain or spinal cord tissue imaging. In both cases, sOBM provides information on tissue morphology complementary to TPEF or CARS contrast. This information is obtained simultaneously and is automatically co-registered. Finally, we show that sOBM can be operated at video rate.

OCIS codes: (110.0180) Microscopy; (180.5810) Scanning microscopy; (290.7050) Turbid media.

References and links

1. J. Pawley, *Handbook of Biological Confocal Microscopy*, 3rd ed. (Springer, 2006).
2. J. G. Fujimoto, "Optical coherence tomography for ultrahigh resolution in vivo imaging," Nat. Biotech. **21**, 1361–1367 (2003).
3. B. R. Masters and P. So, *Handbook of Biomedical Nonlinear Optical Microscopy,* 1st ed. (Oxford Univ. Press, 2008).
4. F. Helmchen, A. Konnerth, and R. Yuste *Imaging in Neuroscience: A Laboratory Manual,* 2nd ed. (CSHL Press, 2011).
5. T. N. Ford, K. K. Chu, and J. Mertz, "Phase-gradient microscopy in thick tissue with oblique back-illumination," Nat. Meth. **9**, 1195–1197 (2012).
6. T. N. Ford and J. Mertz, "Video-rate imaging of microcirculation with single-exposure oblique back-illumination microscopy," J. Biomed Opt. **18**, 0066007 (2013).
7. F. Zernike, "How I discovered phase contrast," Science **121**, 345–349 (1955).
8. G. Nomarski, "Microinterferomètre différentiel à ondes polarisées," J. Phys. Radium **16**, S9 (1955).
9. J. Dodd, "Interferometry with schlieren microscopy," Appl. Opt. **16**, 470–72 (1977).

#201918 - $15.00 USD Received 25 Nov 2013; revised 19 Dec 2013; accepted 19 Dec 2013; published 8 Jan 2014

10. R. Hoffman and L. Gross, "Modulation contrast microscopy," Appl. Opt. **14**, 1169–1176 (1975).
11. H. U. Dodt, M. Eder, A. Frick, and W. Zieglgänsberger, "Precisely localized ltd in the neocortex revealed by infrared-guided laser stimulation," Science **286**, 110–113 (1999).
12. R. Yi, K. K. Chu, and J. Mertz, "Graded-field microscopy with white light," Opt. Express **14**, 5191–5200 (2006).
13. S. B. Mehta and C. J. R. Sheppard, "Quantitative phase-gradient imaging at high resolution with asymmetric illumination-based differential phase contrast," Opt. Lett. **34**, 1924–1926 (2009).
14. B. Kachar, "Asymmetric illumination contrast: a method of image formation for video microscopy," Science **227**, 766–768 (1985).
15. W. T. Welford, "On the relationship between the modes of image formation in scanning microscopy and conventional microscopy," J. Microsc. **96**, 105–07 (1972).
16. M. E. Barnett, "The reciprocity theorem and the equivalence of conventional and transmission microscopes," Optik **38**, 585–588 (1973).
17. D. Kermisch, "Principle of equivalence between scanning and conventional optical imaging systems," J. Opt. Soc. Am. **67**, 1357–1360 (1977).
18. C. J. R. Sheppard and T. Wilson, "On the equivalence of scanning and conventional microscopes," Optik **73**, 39–43 (1986).
19. H. von Helmholtz, *Handbuch der physiologischen Optik,* 1st ed. (Leopold Voss, Leipzig, 1856).
20. Lord Rayleigh, "Some general theorems relating to vibrations," Proc. Lond. Math. Soc. **4**, 357–368 (1873).
21. V. Tuchin, *Tissue Optics: Light scattering methods and instruments for medical diagnosis,* 2nd ed. (SPIE Publications, 2007).
22. W. Denk, J. H. Strickler, and W. W. Webb, "Two-photon laser scanning fluorescence microscopy," Science **248**, 73–76 (1990).
23. S. Komai, W. Denk, P. Osten, M. Brecht, and T. W. Margrie, "Two-photon targeted patching (tptp) in vivo," Nat. Protoc. **1**, 647–52 (2006).
24. K. Kitamura, B. Judkewitz, M. Kano, W. Denk, and M. Ha, "Targeted patch-clamp recordings and single-cell electroporation of unlabeled neurons in vivo," Nat. Meth. **5**, 61–67 (2008).
25. M. Brecht, M. S. Fee, O. Garaschuk, F. Helmchen, T. W. Margrie, K. Svoboda, and P. Osten "Novel approaches to monitor and manipulate single neurons in vivo," J. Neurosci. **24**, 9223-9228 (2004).
26. A. Zumbusch, G. R. Holtom, and X. S. Xie, "Three-dimensional vibrational imaging by coherent anti-Stokes Raman scattering," Phys. Rev. Lett. **82**, 4142–4145 (1999).
27. E. Bélanger, F. P. Henry, R. Vallée, M. A. Randolph, I. E. Kochevar, J. M. Winograd, C. P. Lin, and D. Coté, "In vivo evaluation of demyelination and remyelination in a nerve crush injury model," Biomed. Opt. Express **2**, 2698–2708 (2011).
28. T. Y. P. Chui, D. A. VanNasdale, and S. Burns, "The use of forward scatter to improve retinal vascular imaging with an adaptive optics scanning laser ophthalmoscope," Biomed. Opt. Express **3**, 2537–2549 (2012).
29. C. L. Evans, E. O. Potma, M. Puoris'haag, D. Coté, C. P. Lin, and X. S. Xie, "Chemical imaging of tissue in vivo with video-rate coherent anti-Stokes Raman scattering microscopy," Proc. Natl. Acad. Sci. USA **102**, 16807–16812 (2005).
30. I. Veilleux, J. A. Spenser, D. P. Biss, D. Coté, and C. P. Lin, "In vivo cell tracking with video rate multimodality laser scanning microscopy," IEEE J. Sel. Top. Quantum Electron. **14**, 10–18 (2008).

1. Introduction

Scanning optical microscopy techniques have become enormously popular and can be found in virtually any imaging lab or core facility. Scanning microscopes can exhibit distinct advantages over widefield microscopes, such as an ability to reject out of focus background and provide direct 3D imaging without any numerical post-processing. Optical scanning microscopes applied in biology or biomedical applications are generally based on fluorescence [1], either linear (confocal) or nonlinear (two-photon, etc.). Other varieties of scanning microscopes are based on scattering, either linear (reflection confocal [1], OCT [2]) or nonlinear (SHG, CARS, etc. – see [3]). In all cases, one or more lasers is(are) focused into the sample with an objective, the focal spot(s) is(are) scanned, and the signal is collected with a single element detector such as an avalanche photodiode or photomultiplier tube (PMT). In the case of thick tissue imaging, the signal is collected in an epi-detection geometry through the same objective as the excitation.

With the exception of OCT and reflection confocal (more on these below), scanning microscopes generally offer a degree of specificity, owing for example to a specific fluorophore of interest in the case of fluorescence or to a specific chemical vibration in the case of CARS. While such specificity is useful in most imaging applications, it also presents disadvantages.

#201918 - $15.00 USD Received 25 Nov 2013; revised 19 Dec 2013; accepted 19 Dec 2013; published 8 Jan 2014

In particular, such specificity fails to place the observed signals in context. For example, in the case of fluorescence imaging of cells, only those cells that are labeled are apparent while their unlabeled environments remain dark. In many instances, information about these dark environments can be of interest as it can answer questions such are there other cells nearby? are blood vessels nearby? what is the structure of the local extacellular matrix? etc.. When imaging thin tissue samples, an extra non-fluorescence modality is generally available through some kind of phase contrast technique (see [4]); however when imaging thick tissues most phase contrast techniques fail because they are based on transmission geometries. We introduce an extra imaging modality that can be obtained essentially for free with any scanning microscope. This modality is called scanning Oblique Back-detection Microscopy (sOBM). The main advantages of sOBM are that it requires no tissue labeling and operates in a reflection geometry, meaning it works with arbitrarily thick tissue. Another important advantage of sOBM is its extreme simplicity. It can be implemented as a simple add-on with any standard scanning microscope, commercial or otherwise, without any modifications to the microscope whatsoever. The only requirement is that the microscope possess an available signal input channel.

sOBM is a variant of Oblique Back-illumination Microscopy (OBM), which is a technique to obtain phase contrast in thick tissue using a standard widefield (i.e. camera-based) microscope [5, 6]. Historically, phase contrast imaging is one of the most prevalent applications of widefield microscopy, and there exists an abundance of literature describing different widefield phase contrast techniques. The most common of these are Zernike phase contrast [7] and Normarski differential interference contrast (DIC) [8]. Other techniques include Schlieren microscopy [9], Hoffman contrast [10], Dodt contrast [11] or other variants of oblique field microscopies [12, 13]. As successful as these techniques have been in the lab, they suffer a major drawback: namely they only work in the transmission direction. This limits their application to thin samples only, such as cell monolayers or thin tissue slices. In contrast, OBM works in the epi direction, meaning it can be used with arbitrarily thick tissue.

Standard epi-detection widefield microscopy is based on delivering illumination into the sample through an objective and collecting the resultant signal (fluorescence or otherwise) through the same objective. The only difference between OBM and a standard epi-detection widefield microscope is in the manner in which the illumination is delivered to the sample. Instead of delivering this illumination through the objective, it is delivered by two diametrically opposed off-axis light sources situated just outside the objective housing (see Fig. 1(a)). The illumination undergoes scattering within the tissue, and a portion of it is collected on axis by the objective, ultimately to be imaged by the camera. Because the light sources are situated off axis this collected illumination traverses the focal plane in an oblique manner, thus leading to phase gradient contrast [12, 14]. The advantage of using two light sources instead of a single source is that it allows the acquisition of two sequential images with opposing illumination obliquities. These two images enable the separation of phase contrast from amplitude contrast [13].

It is well known that a scanning microscope is essentially a time-reversed version of a widefield microscope [15–18]. That is, if each pixel in the camera is replaced by an incoherent illumination source turned on sequentially, and the illumination lamp is replaced by a single element detector of equal size, the net result is a scanning microscope. Because of the principle of reciprocity [19], the imaging properties of widefield and scanning microscopes are identical, provided these are linear. This principle remains valid even if the sample is highly scattering or exhibits absorption [20]. sOBM is borne of this principle of reciprocity. sOBM is a time-reversed version of OBM wherein scanning illumination is delivered into the sample via an on-axis objective and, upon back-scattering, is detected by two diametrically opposed off-axis detectors (see Fig. 1(b)). A difference of the two detected signals provides phase gradient contrast; a sum provides amplitude contrast. In the case where the sample presents little absorption,

#201918 - $15.00 USD Received 25 Nov 2013; revised 19 Dec 2013; accepted 19 Dec 2013; published 8 Jan 2014

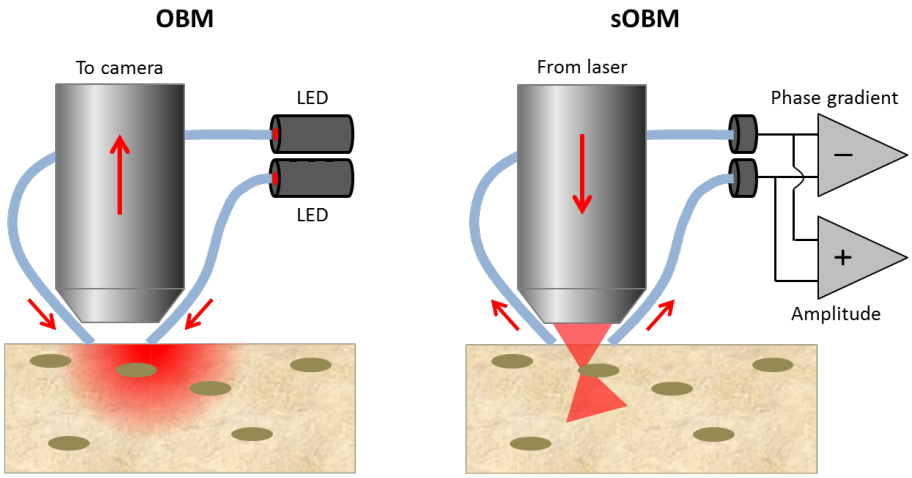

Fig. 1. Schematics of OBM and sOBM setups. In the case of OBM, illumination is delivered into a scattering sample via off axis optical fibers. Oblique backscattered illumination traverses the focal plane and is collected by the microscope objective, whereupon it is ultimately detected by a camera. In the case of sOBM, a scanning laser beam is focused into a scattering sample. The illumination traverses the focal plane and is backscattered, whereupon it is collected by off axis optical fibers and detected by photodiodes. In both cases, the fibers are held flush with the sample surface by a support ring (not shown).

the difference signal is of most interest.

Other scanning microscopy techniques also work in the reflection direction, such as reflection confocal microscopy (RCM) [1]. In RCM, signal arises from local reflectivities in the sample, which, in turn arise from refractive index variations. However, a difficulty with RCM is that scattering structures in most biological tissues are typically micron scale or larger, meaning that scattering is dominantly in the forward direction [21]. Direct backward scattering can only arise from very sharp interfaces or small objects (i.e. refractive index variations with high enough axial spatial frequencies to cause light to reverse its direction), meaning that signal from direct backward scattering is generally weak. Moreover, this signal can be easily overwhelmed by multiply scattered background light containing no image information. Both of these problems are alleviated by optical coherence tomography (OCT), which provides noiseless amplification of directly backscattered signal while rejecting multiply scattered background [2]. Nevertheless, the fact remains that OCT, like RCM, is a reflection technique and inherently reveals only sharp axial interfaces or small structures within samples. In contrast, although sOBM is configured in a reflection geometry, it is actually transmission microscope in disguise, since the illumination is detected *after* it has traversed the focal plane. Thus, sOBM is sensitive to forward scattering and not backward scattering, meaning it is not restricted to imaging only sharp interfaces or small objects, and can instead reveal lower frequency features that are often prevalent in tissue. Compared to OCT, an advantage of sOBM is that it provides images free of speckle noise.

In principle, sOBM can be implemented with any scanning microscope as a simple add-on. We provide examples here where sOBM is combined with TPEF and CARS microscopes, to demonstrate its versatility. Finally, we demonstrate that sOBM can operate even at video rate.

#201918 - $15.00 USD Received 25 Nov 2013; revised 19 Dec 2013; accepted 19 Dec 2013; published 8 Jan 2014

2. sOBM combined with TPEF microscopy

To begin, we demonstrate that sOBM can be implemented with a TPEF microscope [22]. In this case, the TPEF microscope is a commercial device (Prairie Technologies Ultima) built around an upright Olympus BX51 frame with a 40× objective (Olympus LUMPLFL), and a Spectra-Physics Mai Tai excitation laser. No modifications whatsoever were made to this microscope. The sOBM add-on consisted of two bare 1 mm diameter plastic optical fibers (Thorlabs BFL48-1000) held alongside the objective housing with a ring-shaped support, separated by a distance of approximately 8 mm. The support was large enough that the objective could freely move up and down through the ring, allowing unimpeded control of the imaging focal depth. TPEF microscopy was operated in its usual manner. Laser light (810 nm) was focused into the sample to generate fluorescence, which was then epi-collected through the objective and detected within the scan box. In parallel, the operation of sOBM consisted in detecting the laser light itself, specifically the portion of the laser light that underwent backscattering in the sample and was collected off axis by the optical fibers. This light was detected by two PIN photodiodes in a balanced amplified photodetector (Thorlabs PDB210A) of bandwidth (1 MHz) larger than the pixel rate of the TPEF microscope (500 kHz). Only the difference signal was of interest here. This difference signal was then sent through a highpass filter of cutoff frequency 10 kHz chosen to be slower than the pixel rate, but faster than the line-scan rate. The purpose of this highpass filter was twofold. First, it ensured that the difference signal was properly centered about zero, thus compensating for any global mismatch in the fiber collection efficiencies. Second, it corrected for baseline intensity variations associated with beam scanning (this correction is equivalent to the image "flattening" performed on the raw images in standard OBM prior taking their difference). Finally, an overall DC voltage of 2.5 V was added to the filtered difference signal. This last step was necessary because the input channel electronics of the microscope accepted only positive voltages within the range 0–5 V.

Figure 2 shows an example of combined sOBM and TPEF imaging. The sample in this case was a 300 μm slice of GFP-M mouse brain, genetically encoded to sparsely label principal neurons in deep layers of cerebral cortex. The slice was kept thin to facilitate tissue oxygenation. To mimic a much thicker tissue, the slice was supported by a slab of scattering agarose.

Several observations can be made. First, sOBM manifestly provides phase-gradient contrast very similar to standard OBM [5], as predicted by reciprocity, and similar to what would be obtained by DIC in a transmission configuration. This contrast is obtained in parallel with TPEF and is automatically co-registered. In particular, extra-fluorescence sample structure can readily be observed, such as non-fluorescent cells, blood vessels, non-fluorescent neuropil, etc. Another observation is that sOBM provides excellent axial resolution and lateral resolution, on par with TPEF, enabling a clear picture of somatic morphology (see Fig. 2(d)).

This issue of resolution merits closer examination. sOBM is similar to a transmission confocal microscope, but with no detection pinhole. By reciprocity, its resolution performance is equivalent to that of a transmission widefield microscope with essentially Köhler illumination. We thus expect the lateral resolution of sOBM to be diffraction limited for superficial layers in the sample, but to degrade with imaging depth. We have previously shown that the depth penetration of standard OBM is roughly given by the scattering mean free path l_s of light [5]. Again by reciprocity, we expect this to be true of sOBM as well. For brain tissue l_s is roughly 100 μm [21]. Such depth penetration is unfortunately less that can be achieved with TPEF microscopy, meaning that the combination of sOBM and TPEF is expected to be effective only over a limited range. Nevertheless, this range provides access, for example, to cortical layer 2/3 in the juvenile mouse brain for potential in-vivo applications.

With regard to axial resolution, the situation is more interesting. Given that the resolution performance of sOBM is the same as that of a transmission widefield microscope, it might

#201918 - $15.00 USD Received 25 Nov 2013; revised 19 Dec 2013; accepted 19 Dec 2013; published 8 Jan 2014

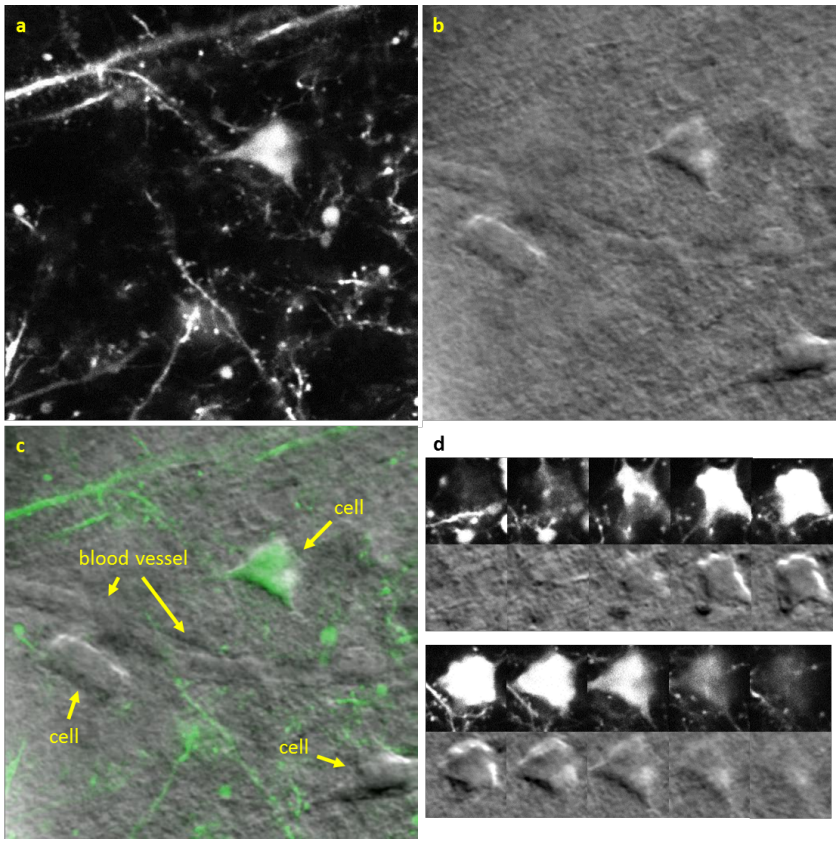

Fig. 2. Simultaneous TPEF (a) and sOBM (b) images of a brain slice of mouse cortex where specific classes of excitatory neurons are genetically labeled with GFP, and overlay (c), taken from a z stack (Media 1 – step size 2 μm). Note non-fluorescent structures revealed by sOBM include unlabeled neurons, dendritic processes receiving synaptic contacts, and a blood vessel. Horizontal processes can be revealed by sOBM but vertical cannot, because of the orientation of the fibers. Focal depth is approximately 30 μm. Field of view is approximately 80 μm. Panel (d) is the z-stack of a representative single fluorescent cell (top right in panel (a)), acquired by TPEF (above) and sOBM (below). Note similar lateral and axial resolutions.

come as a surprise that the axial resolutions of sOBM and TPEF appear to be similar. In fact, a transmission widefield microscope should exhibit very poor axial resolution for large sample structures such as a neuron soma. Why is it that sOBM appears to perform better? The key is that sOBM does not reveal structure itself (here phase) but rather derivatives of structure. Such derivatives inherently contain no low spatial frequencies. It is precisely these low spatial frequencies that widefield microscopes have difficulty axially resolving. Because sOBM images do not contain such low spatial frequencies, axial resolution remains possible, as is manifest in Fig. 2(d).

We note that the picture in Fig. 2(d) is clear enough that it presents a unique possibility for electrophysiologists. Specifically, sOBM may be used to enable the targeted patching of cells completely independently of sample labeling, even in thick tissue where standard transmission-based methods such as IR-DIC [4] or Dodt contrast [11] are impossible. Currently, the only techniques available for targeted patching that are directly compatible with epi-configuration

#201918 - $15.00 USD Received 25 Nov 2013; revised 19 Dec 2013; accepted 19 Dec 2013; published 8 Jan 2014

scanning microscopes are fluorescence based, exploiting either positive [23] or negative [24] contrast. However these techniques are highly specialized and routinely used by only a handful of laboratories. They are also more difficult to use than DIC/Dodt because raw fluorescence images do not offer the same impression of 3D relief as phase-gradient images familiar to electrophysiologists [4, 25].

3. sOBM combined with CARS microscopy

We now demonstrate that sOBM can be implemented with a CARS microscope [26]. In this case, the CARS microscope was based on a commercial beam scanning microscope (Olympus IX71 frame with FV300 scanner). The Stokes beam (1064 nm) was provided by a 80 MHz, 7 ps Nd:Vanadate pulsed laser (picoTRAIN, High Q Laser); the pump beam (817 nm) was provided by a synchronously pumped OPO (Levante Emerald ps, APE), delivering average powers of 3 mW pump and 5 mW Stokes at the sample. The difference frequency was chosen here to resonantly excite the CH_2 symmetric stretch vibrational mode at 2845 cm^{-1}, predominantly a signature of lipids. Both the Stokes and pump beams were superposed with a dichroic filter. A water immersion objective (Olympus LUMPlanFI/IR 40×, 0.8 NA) was used for imaging. The backscattered anti-Stokes signal (662 nm) was collected in the epi-direction and detected by a red-sensitive PMT (Hamamatsu R3896), with pixel rate 100 kHz. The sOBM portion of the microscope was implemented in an identical manner as described above, the only differences being that the microscope geometry was inverted instead of upright, and longpass filters (Edmund Optics 54662, 780 nm) were inserted in front of the balanced photodetectors. These filters played little role aside from assuring that the sOBM signal was free of anti-Stokes signal or possible TPEF fluorescence.

Figure 3 shows representative results. The sample here was an excised slab of spinal cord, approximately 350 μm thick, obtained from a mouse lumbar, and supported by a coverslip. The CARS signal in panels a,c,e predominantly arose from lipid-rich myelin sheaths surrounding nerve axons. These signals have been well characterized, as has the histomorphology of these myelinated axons [27]. Panels b,d,f shows the associated sOBM images, obtained simultaneously. The correspondences between the CARS and sOBM images are striking. As before, the sOBM images resemble DIC-images, though here acquired in an epi-configuration. In addition to revealing lipid-rich myelin sheaths, sOBM also provides an overall survey of sample morphology and texture inaccessible to CARS.

It can be observed that some of the myelinated axons apparent in the CARS images are absent in the sOBM images. These are the axons oriented parallel to the axis separating the sOBM collection fibers. Indeed, sOBM reveals only phase gradients parallel to the optical fiber separation axis. As such, it reveals only myelinated axons perpendicular to this axis. An easy remedy to this problem is to include two additional detection fibers in our sOBM setup, along with associated electronics. This is planned as a future development.

There also remains the question of optimal fiber placement. It was shown in Ref. [5] that the signal in standard OBM is relatively insensitive to fiber placement, though it increases somewhat with decreasing fiber separation. By reciprocity, we expect the same to be true of sOBM. In our experiments we kept the fiber separation to a minimum while keeping the fibers outside the objective housing. One may wonder if better performance could have been achieved by placing detectors effectively inside the objective housing rather than outside. For example, could offset detectors (e.g. see [28]) have been placed internal to the microscope hardware that provided signal collection from just outside the microscope field of view? Our initial attempts at this were unsuccessful and yielded instead a decrease in sOBM contrast, presumably arising from the spurious detection of background light directly scattered from the sample surface. Also, it should be noted that such a strategy of modifying the microscope internal hardware

#201918 - $15.00 USD Received 25 Nov 2013; revised 19 Dec 2013; accepted 19 Dec 2013; published 8 Jan 2014

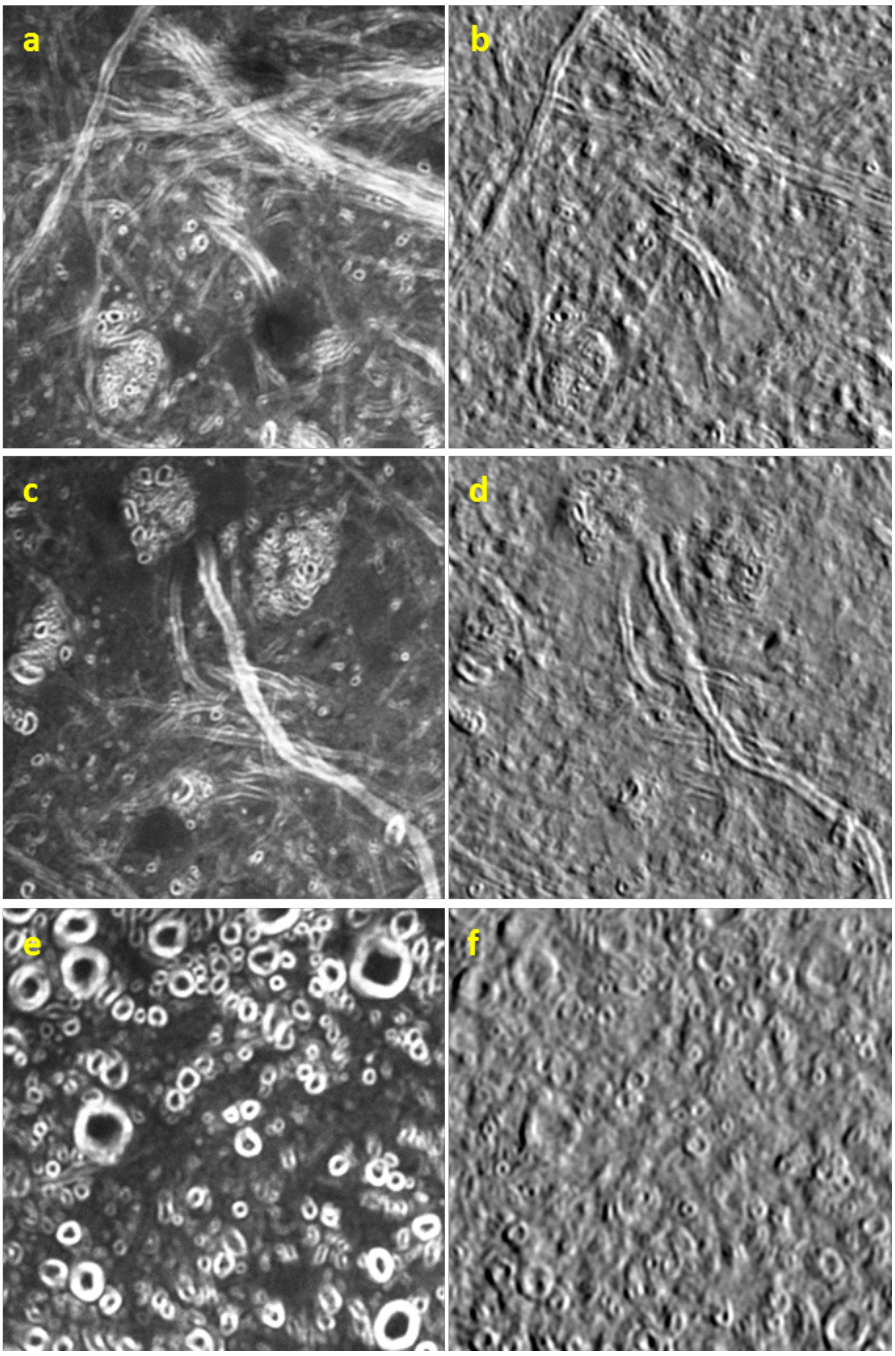

Fig. 3. Simultaneous CARS (left) and sOBM (right) images of a cross-sectional cut of a mouse spinal cord from lumbar region. The CARS signal arose mostly from lipid-rich myelin sheaths surrounding nerve axons. Note correspondence between CARS and sOBM images. Focal depth was approximately 10 μm. Field of view was (a–d) 78 μm and (e,f) 55 μm.

#201918 - $15.00 USD Received 25 Nov 2013; revised 19 Dec 2013; accepted 19 Dec 2013; published 8 Jan 2014

undermines an attractive feature of sOBM that it can be implemented as a simple add-on that leaves the intended function of the microscope unchanged.

4. Video-rate sOBM

In previous work, we have shown that standard OBM can operate at video rate. Here, we show that the same is true of sOBM. For this, we used a video rate scanning microscope designed for CARS microscopy [29, 30], but applied here simply for sOBM. The illumination source was the same as described above, but here only the pump beam (817 nm) was used, delivering roughly 50 mW to the sample through a water-immersion objective (Olympus LUMPlanFI/IR 40×, 0.8 NA). Beam scanning was performed by a spinning polygonal mirror (Lincoln Laser: DT-36-290-025, 36 facets) to produce a fast unidirectional scan along the horizontal axis, and a galvanometer mounted mirror (Cambridge Technology: 6240H) to produce the slower scan along the vertical axis. The polygonal mirror rotated at 480 revolutions/s, thereby delivering a line scanning rate of 17280 Hz (36×480), which, at a frame rate of 30 Hz, corresponds to 576 lines per image. The pixel rate of this microscope was 13.175 MHz, corresponding to 752 pixels per line.

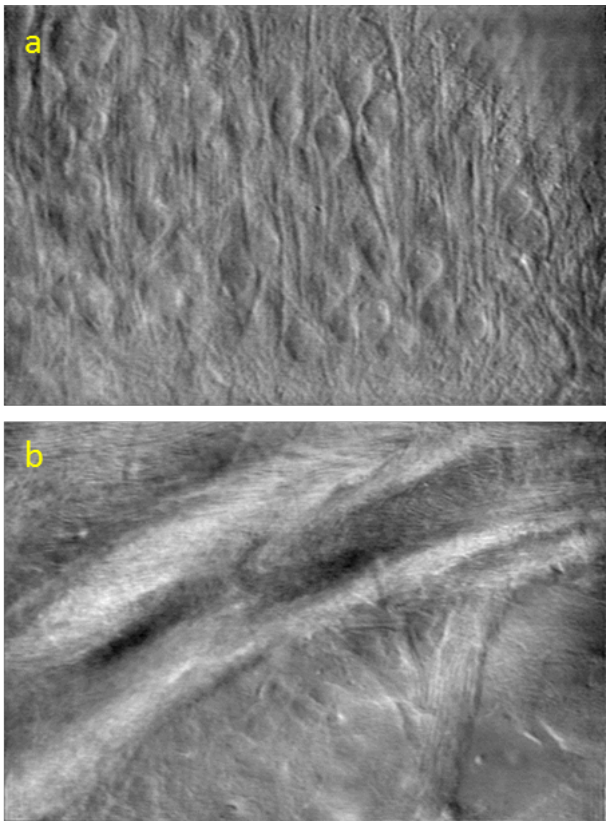

Fig. 4. Images of a coronal section of mouse brain acquired by video-rate sOBM. Panel (a) reveals cell bodies from gray matter; panel (b) reveals axon tracts likely to be myelinated. Focal depth was approximately 10μm. Field of view was approximately 254 × 159 μm.

Because the pixel rate of this microscope was much faster than could be handled by the electronics of our balanced photodetector, we instead made use of the internal detectors in the

#201918 - $15.00 USD Received 25 Nov 2013; revised 19 Dec 2013; accepted 19 Dec 2013; published 8 Jan 2014

microscope for the implementation of sOBM. That is, we routed the proximal ends of of the sOBM collection fibers into the microscope detector modules containing red-sensitive PMTs (Hamamatsu R3896). Only two channels were available, normally dedicated to the detection of anti-Stokes and simultaneous TPEF signal. Here, the channels provided sOBM signal from the two detection fibers. As such, there was no possibility to combine sOBM with an additional contrast. Moreover, sOBM image processing had to be performed a posteriori, in a manner similar to the processing performed with standard OBM. That is, the raw images obtained by each channel were numerically flattened and normalized post acquisition, and then subtracted for phase-gradient contrast (or added for amplitude contrast).

Figure 4 provides representative phase-gradient sOBM images acquired at video rate. The sample in this case was a 1 mm thick coronal section through the corpus collusum of a mouse (C57BL/6). Again, these images resemble DIC images. Their quality is manifestly not as high as those in Fig. 3. Several reasons may explain this. First, the index of refraction variations within brain tissue (the source of sOBM contrast) are likely to be intrinsically weaker than those in the spinal cord. Second, much less light was delivered to the sample per exposure time, by about a factor of 20, meaning that the signal to noise ratio was likely to be compromised. Third, the dynamic range of our video-rate sOBM was much less than that of our non-video-rate systems because the raw images were 8-bit digitized in our video-rate system prior to being subtracted, whereas subtraction was performed prior to digitization in our non-video-rate systems. Nevertheless, despite the deficiencies of our video rate system, video rate sOBM remained possible and, indeed, effective. In future developments we will modify our balanced photodiode electronics to be fast enough to allow video rate sOBM in real time.

5. Conclusion

In summary, we have made use of the principle of reciprocity to introduce a time-reversed variant of standard OBM. This variant may be applied as an add-on to any scanning microscope. We have limited our demonstrations here to TPEF and CARS microscopes, though sOBM is equally compatible with other types of epi-configuration scanning microscopes, such as fluorescence or reflectance confocal, OCT (time domain), SHG, etc.. Given the simplicity and cost-effectiveness of sOBM, and the fact that it imposes no modifications on the scanning microscopes whatsoever, the extra information provided by sOBM comes essentially for free. As such, sOBM is an attractive technique for obtaining complementary image contrast.

Acknowledgements

We thank Yves De Koninck for discussions and helpful support. This work was aided by NIH grant R01-EB010059.

#201918 - $15.00 USD Received 25 Nov 2013; revised 19 Dec 2013; accepted 19 Dec 2013; published 8 Jan 2014